In situ ohmic contact formation for n-type Ge via non-equilibrium processing

Prucnal, S.; Frigerio, J.; Napolitani, E.; Ballabio, A.; Berencén, Y.; Rebohle, L.; Wang, M.; Böttger, R.; Voelskow, M.; Isella, G.; Hübner, R.; Helm, M.; Zhou, S.; Skorupa, W.;

Originally published:

October 2017

Semiconductor Science and Technology 32(2017), 115006

DOI: https://doi.org/10.1088/1361-6641/aa8b2f

In-situ ohmic contact formation for n-type Ge via non-equilibrium processing

S. Prucnal[1,a)], J. Frigerio[2], E. Napolitani[3], A. Ballabio[2], Y. Berencén[1], L. Rebohle[1], M. Wang[1], R. Böttger[1], M. Voelskow[1], G. Isella[2], R. Hübner[1], M. Helm[1], S. Zhou[1] and W. Skorupa[1]

[1] *Helmholtz-Zentrum Dresden-Rossendorf, Institute of Ion Beam Physics and Materials Research, Bautzner Landstraße 400, D-01328 Dresden, Germany*

[2] *L-NESS, Dipartimento di Fisica, Politecnico di Milano, Polo di Como, Via Anzani 42, I-22100 Como, Italy*

[3] *Dipartimento di Fisica e Astronomia, Università di Padova and CNR-IMM MATIS, Via Marzolo 8, I-35131 Padova, Italy*

Abstract

Highly scaled nanoelectronics requires effective channel doping above 5×10^{19} cm^{-3} together with ohmic contacts with extremely low specific contact resistivity. Nowadays, Ge becomes very attractive for modern optoelectronics due to the high carrier mobility and the quasi-direct bandgap, but n-type Ge doped above 5×10^{19} cm^{-3} is metastable and thus difficult to be achieved. In this letter, we report on the formation of low-resistivity ohmic contacts in highly n-type doped Ge via non-equilibrium thermal processing consisting of millisecond-range flash lamp annealing. This is a single-step process that allows for the formation of a 90-nm-thick NiGe layer with a very sharp interface between NiGe and Ge. The measured carrier concentration in Ge is above 9×10^{19} cm^{-3} with a specific contact resistivity of 1.2×10^{-6} Ωcm^2. Simultaneously, both the diffusion and the electrical deactivation of P are fully suppressed.

Keywords: Ge, flash lamp annealing, ion implantation, ohmic contact, NiGe

[a)]Electronic mail: s.prucnal@hzdr.de

Introduction

Electronic and structural properties of Si were sufficient to fulfil the requirements of microelectronic industry for more than five decades. Further progress via miniaturisation of transistors is challenging. Therefore, the improvement of the transistor performance can be realised alternatively by e.g. the increase of charge-carrier mobility within the channel [1-4]. In fact, the first transistor was made of Ge and today Ge has the chance for a great comeback. Ge is chemically similar to Si but the electron and hole mobilities in Ge is two and four times higher than those of Si, respectively. The key challenges for high-performance Ge-based nanoelectronics are: (i) the fabrication of highly-doped and stable *p*- and *n-type* channel material and (ii) low-resistance ohmic contacts [3].

Donors in Ge are fast diffusers and the equilibrium solid solubility limit is slightly above 10^{20} cm^{-3} for P and in the range of 2 to 3×10^{19} cm^{-3} for As and Sb [5-7]. However, the active carrier concentration in n-type Ge fabricated using equilibrium methods is limited to 3×10^{19} cm^{-3} [4]. A doping level above 10^{20} cm^{-3} can be achieved in Ge by applying non-equilibrium methods which enable donor activation, e.g. nanosecond-range laser melting [8], molecular beam epitaxy (MBE) using *in-diffusion* with a δ–doped layer [9], ion implantation followed by millisecond-range flash lamp annealing (FLA) [4, 10] or multistep ion implantation followed by rapid thermal annealing (RTA) [11]. However, ultra-doped n-type Ge is metastable and additional thermal treatments, for instance, during the ohmic contact formation, deactivate donors to the equilibrium level ($n_e=3\times10^{19}$ cm^{-3}). R. Milazzo *et al.* have investigated the influence of low-temperature thermal treatment on the deactivation of carriers in Ge doped with As via ion implantation and nanosecond laser melting with an active carrier concentration above 1×10^{20} cm^{-3} [12]. They have shown that annealing at 350 ^{o}C reduces the active carrier concentration in As-doped Ge to 4×10^{19} cm^{-3}. After annealing at 450 ^{o}C the active carrier concentration further decreases to 3×10^{19} cm^{-3}.

To this day, one of the lowest ever published specific contact resistivities (ρ_c) between NiGe and n-type Ge ($n_e = 3\times10^{19}$ cm^{-3}) was reported for orthorhombic NiGe made by low-temperature germanidation at 340 ^{o}C ($\rho_c = 2.3\times10^{-7}$ Ωcm^2) [13]. Using nanosecond-pulsed laser annealing, Huang *et al.* have shown a specific contact resistivity as low as 1.6×10^{-8} Ωcm^2 before and 1.5×10^{-8} Ωcm^2 after germanidation with nanosecond pulsed laser annealing [8] which, however, is not industry relevant. According to the International Technology Roadmap for Semiconductors (ITRS), the specific contact resistivity for both n- and p-type

Ge should be below 10^{-7} Ωcm^2. Therefore, various sophisticated approaches are carried out to meet the ITRS requirements [14-16].

In this letter, we present *in-situ* low-resistance ohmic contact formation in highly doped n-type Ge with an active carrier concentration above 1×10^{20} cm^{-3}. The NiGe layer for ohmic contact formation and the activation of P are done by single-step rear-side flash lamp annealing. During 20 ms FLA pulse, Ni of a 50 nm thick layer diffuse into Ge forming an about 90 nm thick NiGe layer with very sharp interface. Moreover, due to the ultra-high n-type doping, Ge becomes a quasi-direct band gap semiconductor showing room-temperature photoluminescence (RT-PL) from Γ-HH transitions. The presented RT-PL peak position is red-shifted by more than 200 nm with respect to Γ-HH transitions observed from lightly-doped Ge.

Experiment

400 nm thick Ge layers were grown epitaxially on (100) Si substrates by low-energy plasma enhanced chemical vapour deposition (LE-PECVD). Details about the LE-PECVD working principle can be found in Ref. 17. Basically, the single crystalline Ge epilayers were grown at 500^{o}C at a rate of ~1 nm/s using GeH_4 as precursor. N-type doping of Ge was realised by adding PH_3 molecules into the reactor chamber with a gas flow of 0.35 sccm. In the as-grown layer, the maximum effective carrier concentration is around 2.3×10^{19} cm^{-3}, while the incorporated P concentration in Ge is in the range of $1\text{-}2\times10^{20}$ cm^{-3}. After depositing the crystalline Ge layer, millisecond-range FLA was performed. Ge samples were annealed from the rear side for 3 or 20 ms with an energy density ranging from 50 to 140 Jcm^{-2} [4]. In our FLA system (FLA200), during single flash eight inch wafer can be homogeneously annealed with maximum temperature easily exciding melting point of Ge or Si. The flash is performed with the bank of twelve 26 cm long Xe lamps with the emission spectrum covering UV-visible spectral range (320 – 850 nm). We also investigated the influence of the pre-amorphisation of the doped layer on the carrier concentration and P distribution after FLA. To this end, Ge ions were implanted into the as-grown layer with a fluence of 1×10^{15} cm^{-2} at an energy of 230 keV which leads to the formation of an about 250 nm thick amorphous Ge layer. Prior to the ion implantation, a 30 nm thick SiO_2 layer was deposited to prevent the Ge surface from roughening during ion implantation. The SiO_2 layer was removed after annealing in a buffered hydrofluoric acid. Ohmic contacts were formed by depositing a 50 nm thick Ni layer on either as-deposited or pre-amorphised Ge and millisecond-range germanidation process. In such a case P activation and NiGe formation is performed during single annealing

step. The main advantage of FLA over conventional annealing is that during a single flash pulse Ni diffuses into Ge, the amorphous Ge layer recrystallizes epitaxially, P is electrically activated while P diffusion is fully suppressed.

The crystalline quality of FLA-treated Ge and the distribution of Ni in Ge were studied using Rutherford backscattering spectrometry in channelling (RBS/C) and random (RBS/R) direction. The RBS/C and RBS/R measurements were performed on the samples before and after annealing using the 1.7 MeV He^+ beam of the Rossendorf van de Graff accelerator. To investigate the microstructural properties of the NiGe layer, cross-sectional bright-field and high-resolution transmission electron microscopy (TEM) investigations were performed in a Titan 80-300 (FEI) microscope operated at an accelerating voltage of 300 kV. High-angle annular dark-field scanning transmission electron microscopy (HAADF-STEM) imaging and element mapping based on energy-dispersive X-ray spectroscopy (EDXS) were performed at 200 kV with a Talos F200X microscope equipped with a Super-X EDXS detector system (FEI). Prior to TEM analysis, the specimen mounted in a high-visibility low-background holder was placed for 10 s into a Model 1020 Plasma Cleaner (Fischione) to remove organic contamination. The distribution of P in Ge was measured by SIMS. The activation efficiency of P in Ge was determined by Hall Effect measurements using a commercial Lakeshore Hall System HMS 9709A with the van der Pauw geometry. The Hall Effect measurements were performed in the temperature range from 2.5 to 300 K. The measurements of contact resistance were carried out using the transfer length method (TLM). 200 μm long × 50 μm wide Ni stripes separated by 10, 20, 40, 60, 80 and 100 μm were deposited on Ge using optical lithography and lift-off. The TLM structures allow to one extract the contact resistance (R_c), transfer length (L_T), and sheet resistance (R_s) from which the specific contact resistance (ρ_c) is subsequently calculated. Photoluminescence (PL) and micro-Raman spectroscopy were used to study the optical properties of the fabricated Ge and NiGe films. In both cases, a 532-nm-laser was used for the excitation. The PL signal was detected by a InGaAs detector.

Results and discussion

Optical properties of ultra-doped n-type Ge were investigated by μ-Raman and PL spectroscopy. Figure 1a shows μ-Raman spectra obtained from an *in-situ* P-doped Ge layer grown epitaxially on Si after amorphisation and FLA. Due to the limited penetration depth of the 532 nm laser in Ge (viz. ~50 nm), the as-implanted sample exhibits only a broad band at about 275 cm^{-1} originating from the amorphous film created during the ion implantation process. The as-grown and FLA-treated samples show narrow peaks at 300.3 and 299.7 cm^{-1},

respectively. According to the Raman spectra, the as-grown Ge layer is fully relaxed while the flash lamp annealed one is tensile strained. Quantitative analysis of the in-plane strain in the fabricated layers can be inferred according to $\varepsilon=[\Delta\omega/c]100\%$, where, $\Delta\omega$ is the shift of the phonon mode position and *c* is a pre-factor (~ -408 for Ge) [18]. With $\Delta\omega=(-0.6 \pm 0.1)$ cm^{-1} and c = -408, the implanted and subsequently FLA-treated Ge layer has a tensile strain of around (0.14±0.02)%. Raman spectroscopy can be also used to inspect the activation efficiency of P in Ge. The Ge-P molecule has a Raman-active phonon mode located at about 340 cm^{-1} and the peak position depends on the P concentration incorporated into the lattice [19].

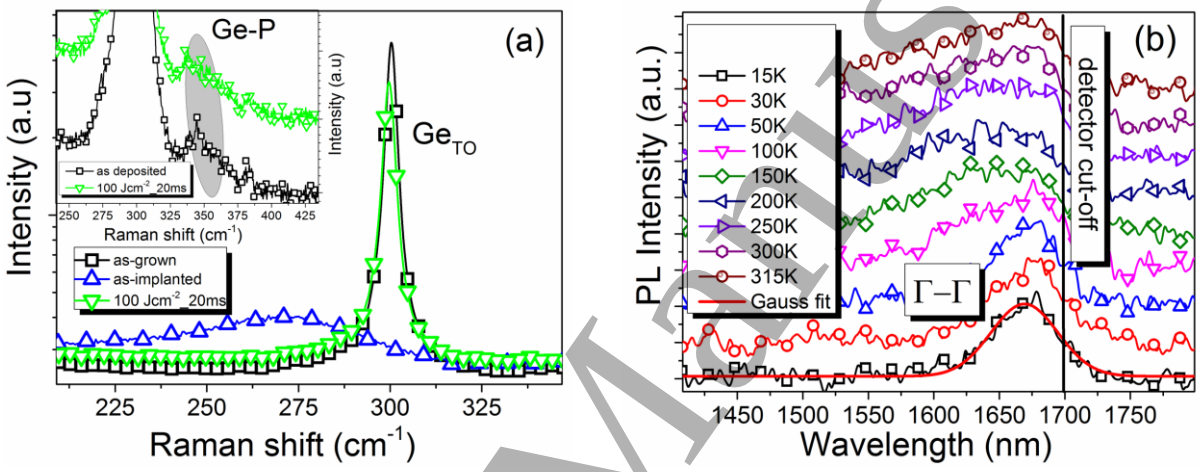

Figure 1. (a) Micro-Raman spectra obtained (i) after LE-PECVD growth of the Ge layer (as-grown), (ii) after Ge ion implantation (as-implanted), and (iii) subsequent FLA treatment at 120 Jcm^{-2} for 20 ms. The inset shows the magnified spectrum range of 240 – 430 cm^{-1}. (b) temperature-dependent photoluminescence (TD-PL) spectrum obtained from the FLA-treated Ge-film (120 Jcm^{-2} for 20 ms). Spectrum fitting was done with Gaussian curve representing the Γ–Γ direct transition at a peak position of 1670 nm at 15K.

The peak position of the Ge-P phonon mode shifts towards smaller wavenumbers with increasing concentration of Ge-P bonds, i.e. electrically active P atoms. In our case, the concentration of electrically active P in as-grown Ge is in the range of 2.3×10^{19} cm^{-3} which corresponds to a phonon mode position of 344 cm^{-1} (see inset Fig. 1a). After FLA the Ge-P phonon mode shifts to 337 cm^{-1} corresponding to an increase of the active carrier concentration to 9×10^{19} cm^{-3} [19]. Tensile strain together with n-type doping in the range of 10^{20} cm^{-3} can induce a change of the Ge band gap from indirect to quasi-direct, which makes Ge attractive for optoelectronic applications. It was shown that the lowest tensile strain required for the quasi-direct band gap formation in Ge is 1.9 % [20, 21]. However, it can be

significantly reduced by the proper combination of tensile strain and ultra-high n-type doping. Even in relaxed Ge films with sufficiently high electron concentrations the direct transition can dominate the PL emission. Figure 1b shows the temperature-dependent PL spectrum obtained from a n-type Ge layer after amorphisation and FLA treatment at 120 Jcm^{-2} for 20 ms. The 1670 nm PL emission recorded at 15 K corresponds to the direct radiative recombination of electrons and holes at the Γ point. For such heavily doped n-type Ge the RT Γ–Γ direct transition is expected at 1720 nm but [22] it is not fully recorded due to the detector cut-off. In the temperature range from 15 to 320 K the peak intensity of the direct transition increases with increasing temperature due to an enhancement of the population of the Γ valley by electrons which recombine with holes via a direct transition [23]. For the tensile strained layers in the range of 0.25%, the energy difference between the Γ valley and the L valley is about 115 meV, which can be compensated by n-type doping with an electron concentration higher than 7.6×10^{19} cm^{-3} [22, 23]. In our case, the tensile strain is lower (0.14 %), but the effective carrier concentration is in the range of 9×10^{19} cm^{-3} and with these values the Fermi level lies only 3 meV below the bottom of the Γ valley and the relative population ratio between the Γ and L valleys electrons is 1.7×10^{-3}, which is one order of magnitude higher with respect to the as-grown sample [24]

The crystalline quality and the P distribution within the fabricated Ge-on-Si films after ion implantation and FLA were investigated by RBS (see Fig. 2a) and SIMS (see Fig. 2b), respectively. The RBS/C yield recorded at the surface of Ge drops down below 8% (channel 760) compared to the RBS/R signal both before and after FLA (see Fig. 2a), indicating a good crystal quality of the layer. The slight decrease of the RBS/C yield close to the Si/Ge interface after FLA suggests a reduction of the density of threading dislocations and point defects. Regarding the quality of the Si/Ge interface no differences between the implanted and the non-implanted samples are observed after FLA in the RBS/C spectra (see Fig. 2a). RBS/C and RBS/R were also used to determine the thickness of the amorphous layer (about 250 nm) formed during ion implantation and the thickness of the NiGe layer (about 90 nm) created during FLA (not shown here). After 20 ms annealing the 50 nm thick Ni is completely converted into NiGe. After germanidation for 3 ms, only 30 nm of Ni was converted into NiGe. Figure 2 b shows SIMS data obtained from an as-grown, an annealed but not implanted and from an implanted sample followed by FLA. The samples were annealed for 20 ms from the rear side with an energy density of 100 Jcm^{-2} which corresponds to a peak surface temperature of about 850 ^{o}C. The P atoms are relatively homogeneously distributed over the

layer thickness at a concentration of about 1.5×10^{20} cm^{-3}. As shown by Hall measurements, the carrier concentration in the as-deposited sample is limited to 3×10^{19} cm^{-3}.

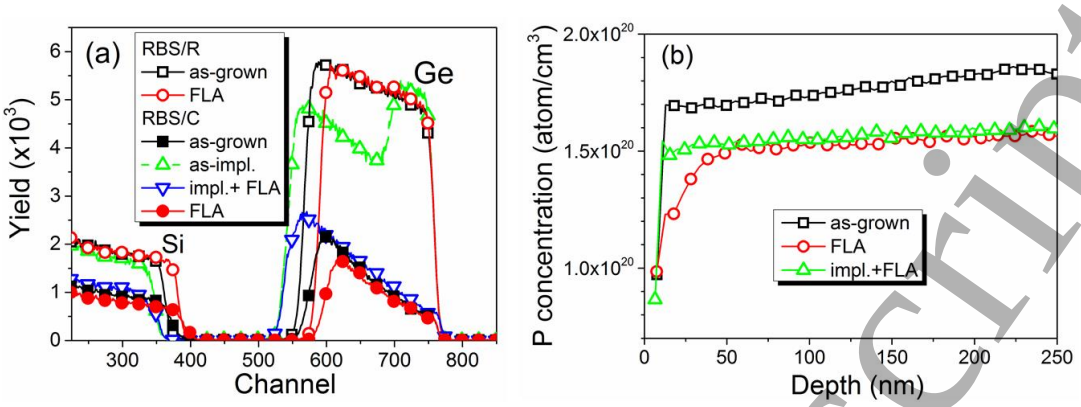

Figure 2. (a) RBS random (RBS/R) and channeling (RBS/C) spectra obtained before and after FLA (b) P distribution in the Ge layer before and after FLA obtained by SIMS. FLA was performed for 20 ms with an energy density of 100 Jcm^{-2}.

After FLA for 20 ms without amorphisation, the effective carrier concentration increases up to 9×10^{19} cm^{-3} but P atoms partially out-diffuse from the surface region. The sample amorphised by ion implantation and subsequently flash lamp annealed shows the same carrier concentration but the out-diffusion of P is suppressed (see Fig. 2b). Hence the SiO_2 layer deposited to prevent the surface roughening during ion implantation is also useful to avoid the out-diffusion of P during the FLA process.

Figure 3 a shows a cross-sectional bright-field TEM image obtained from a Ge-on-Si wafer with 50 nm Ni stripes after FLA for 20 ms. After the growth sample surface is flat. Moreover, during Ni deposition samples were not intentionally heated, so, at this step, the diffusion of Ni into Ge and roughening of the Ni/Ge interface is not expected. As indicated by the laterally varying diffraction contrast in the upper layer of the stack, flash lamp annealing leads to the formation of a polycrystalline Ni germanide with a grain size in the order of 200 nm. The interface to germanium appears sharp but wavy (Fig. 3 a). It is the latter fact which is causing the Moiré patterns as seen in Figure 3 b at the interface between the crystals of Ni germanide and germanium. To further characterize the structure of the Ni germanide, Fourier transform analysis of the corresponding region in the high-resolution TEM image was performed. The main peaks in the Fast Fourier Transform (FFT, upper inset of Fig. 3b) correspond to an [110] zone axis pattern of orthorhombic NiGe [25]. The stoichiometry of the fabricated NiGe layer was further investigated by mapping the Ni and Ge element distributions based on energy-dispersive X-Ray spectroscopy (EDXS) in scanning TEM (STEM) mode (see Figs 3 c-e).

Figure 3 e shows superimposed distribution of Ni and Ge after germanidation during FLA. Within the NiGe layer, both elements are homogeneously distributed. Quantitative analysis reveals Ni concentrations between 50 and 53 at.-%. It should be mentioned that small $Ni_{0.60}Ge_{0.40}$ clusters were found additionally. They are hemispherically shaped and located close to the sample surface with an average lateral size on the order of 50 to 100 nm and an approximate height of 40 nm. Since the density of such clusters is low, (viz. four $Ni_{0.60}Ge_{0.40}$ clusters were found in one TEM window of 5 µm width), no significant influence on the electrical properties of the ohmic contacts is expected.

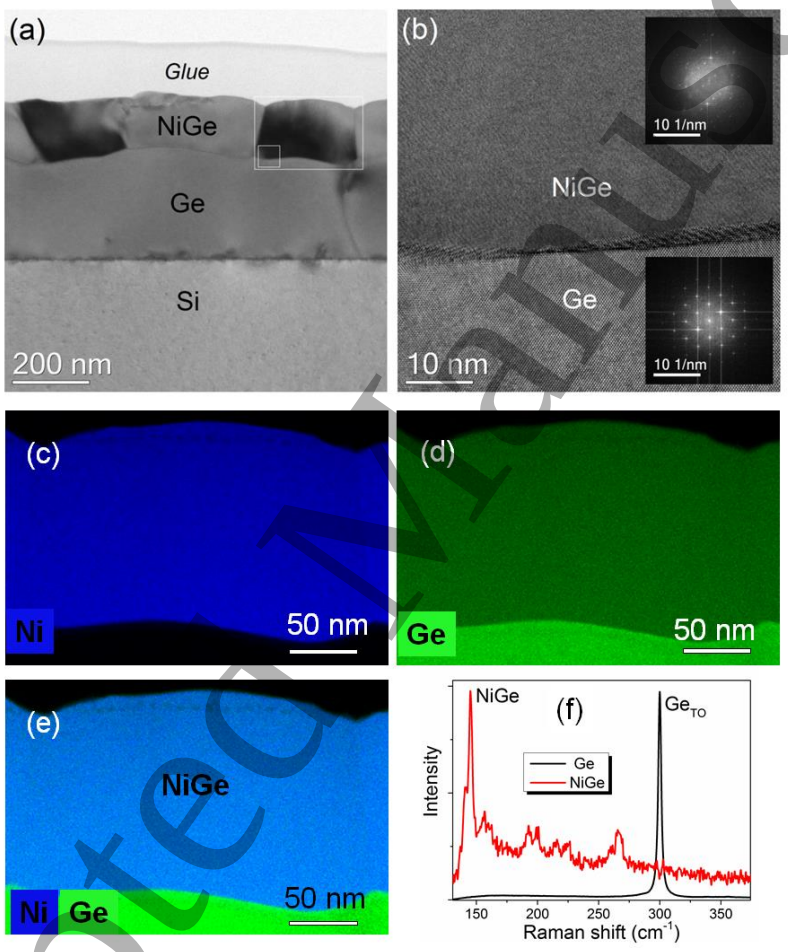

Figure 3. (a) Cross-sectional bright-field TEM image of a 50 nm thick Ni layer deposited onto a Ge-on-Si wafer after FLA for 20 ms. (b) High-resolution TEM image of the interface region between NiGe and Ge as marked by the white square in (a). The upper and lower inset represent Fast Fourier Transforms (FFT) of the NiGe and the Ge regions, respectively. (c) Ni (blue) element distribution, (d) Ge (green) element distribution and (e) superimposed Ni and Ge element distributions based on EDXS obtained in scanning TEM mode for the region

marked by the white rectangle in (a), respectively. (f) μ-Raman spectra of NiGe (red) and Ge layer (black).

The interface between NiGe and germanium is sharp. In particular, no inter-diffusion layer with varying Ni concentration is observed (Fig. 3c). The formation of orthorhombic NiGe was also confirmed by μ-Raman measurements (see Fig. 3f). The Raman spectrum exhibits distinct peaks at 140 and 145 cm^{-1} accompanied by smaller features at 156, 192, 224 and 266 cm^{-1}. The Raman active phonon modes in relaxed (100) NiGe are expected to be located at 140, 194 and 217 cm^{-1} [26]. The shift of the phonon modes towards higher wavenumbers suggests the existence of compressive strain (phonon modes observed at 146 and 224 cm^{-1}). This is expected since the lattice parameters of orthorhombic NiGe are smaller than the lattice parameter of cubic Ge. Moreover, the shift of the phonon mode peak position can be caused by the polycrystalline nature of the fabricated NiGe films. It seems that during the first step of the germanidation process the intermediate Ni_xGe_y becomes liquid that subsequently solidifies by random nucleation of NiGe grains. Taking into account the phase diagram of Ni_xGe_y and the maximum temperature during FLA process (~850 ^oC), the Ni_2Ge phase is likely formed at first since it has the lowest melting temperature (~506 ^oC) among other nickel germanide phases [27]. When the temperature of the nickel germanide layer increases above 550 ^oC, the Ni_2Ge is reduced to stoichiometric NiGe which undergoes solidification immediately (melting point higher than 850 ^oC).

The electrical properties of the NiGe/n-type Ge system were evaluated using the TLM. Figure 4a shows exemplarily the current-voltage (I-V) characteristics obtained at room temperature between two contacts spaced by 40 μm for samples directly after Ni deposition and after FLA for 3 and 20 ms. The linear behaviour of the I-V curves proves the ohmic contact formation between the metal contact and the n-type Ge. In order to extract ρ_c, the measured resistance R was plotted as a function of contact spacing (see Fig. 4b). The linear fit of the data points allows calculating the transfer length L_T and the contact resistance R_C. Additionally, the sheet resistance (R_{Sh}) and ρ_c can respectively be calculated by the following expressions: $R_{Sh} = \frac{R_C W}{L_T}$, and $\rho_C = R_{Sh} L_T^2$, where W is the length of NiGe stripes. The influence of the annealing time on the total resistance as a function of gap spacing is shown in Fig. 4b. The energy density of flash lamp was adjusted for each annealing time in order to maximize the carrier concentration (see Table 1). According to our experiments, flash-lamp energy densities around 90 Jcm^{-2} and below are not sufficient to fully recrystallize the pre-amorphized Ge layer. On the contrary, the samples are molten at flash-lamp energy densities higher than 110

Jcm^{-2}. In addition, without the preamorphization step, flash-lamp annealed Ge samples at energy densities of 90 Jcm^{-2} for 20 ms exhibit carrier concentrations very similar to that of the as-grown samples.

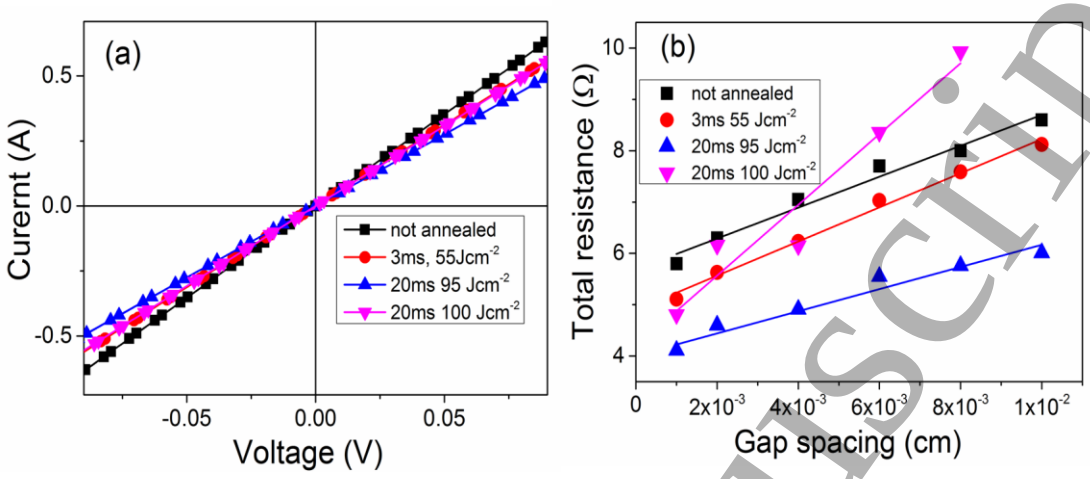

Figure 4. (a) Current-voltage (I-V) characteristics obtained from TLM and (b) the total resistance as a function of gap spacing for TLM.

According to Hall Effect measurements, the maximum carrier concentration was estimated to vary between 0.9 and 1×10^{20} cm^{-3} for 20 ms annealed samples with an energy density between 95 and 100 Jcm^{-2}, respectively. After annealing for 3 ms, the maximum carrier concentration was found to be in the range of 4-5×10^{19} cm^{-3}. At the same time, ρ_c varied between 1.2×10^{-6} Ωcm^2 and 5.1×10^{-6} Ωcm^2 for the flash lamp annealed sample for 20 ms and the not annealed sample, respectively.

Table 1. Carrier concentration (n_e) and specific contact resistance (ρ_c) obtained from TLM for optimized annealing parameters.

FLA time (ms)	FLA (Jcm^{-2})	n_e (cm^{-3})	R_{sh} (Ωsq)	L_T (cm)	ρ_c (Ωcm^2)
–	–	2.0±0.5×10^{19}	0.061	9×10^{-3}	5.10×10^{-6}
3ms	55	4.5±0.5×10^{19}	0.66	7×10^{-3}	3.43×10^{-6}
20ms	95	9.0±0.5×10^{19}	0.043	9×10^{-3}	3.60×10^{-6}
20ms	100	1.0±0.5×10^{20}	0.13	3×10^{-3}	1.20×10^{-6}

Conclusions

A non-equilibrium thermal process via millisecond-flash lamp annealing is successful to activate P in Ge layers and to form ohmic contacts with a specific contact resistivity as low as

1.2×10^{-6} Ωcm^2. The maximum carrier concentration was measured to be in the range of 10^{20} cm^{-3}. It was also found that an annealing time of 20 ms is sufficient to fully convert 50 nm thick Ni to 90 nm thick Ni germanide. The fabricated ohmic contacts are polycrystalline with very sharp interface between NiGe and Ge. This single-step approach has also the advantage of suppressing the unwanted diffusion of P and its electrical deactivation traditionally observed after conventional post-deposition annealing treatment.

Acknowledgement

Support by the Ion Beam Center (IBC) at HZDR is gratefully acknowledged. We would like to thank H. Hilliges, A. Kunz, and B. Scheumann from HZDR for careful sample preparation. Funding of TEM Talos F200X by the German Federal Ministry of Education of Research (BMBF), Grant No. 03SF0451 in the framework of HEMCP is gratefully acknowledged. Y. Berencén would like to thank the Alexander-von-Humboldt foundation for providing a postdoctoral fellowship. The research leading to these results has received funding from the European Union's Seventh Framework Programme under grant agreement no. 613055

References:

1. Weber W M and Mikolajick T 2017 *Rep. Prog. Phys.* **80,** 066502.
2. Chau R, Doyle B, Datta S, Kavalieros J and Zhang K 2007 *Nature Materials* **6**, 810 - 812.
3. Kamata Y 2008 *Materials Today* **11**, 30-38.
4. Prucnal S, Liu F, Voelskow M, Vines L, Rebohle L, Lang D, Berencén Y, Andric S, Boettger R, Helm M, Zhou S and Skorupa W 2016 *Sci. Rep.* **6**, 27643.
5. Goley P S and Hudait M K 2014 *Materials* **7**, 2301-2339.
6. Impellizzeri G, Boninelli S, Priolo F, Napolitani E, Spinella C, Chroneos A and Bracht H 2011 *J. Appl. Phys.* **109**, 113527.
7. Weber J R, Janotti A and Van de Walle C G 2013 *Phys. Rev. B* **87**, 035203.
8. Huang S.-H, Lu F.-L, Huang W.-L, Huang C.-H and Liu C W 2015 *IEEE Electron Device Lett.*, **36**, 1114.

9. Mattoni G, Klesse W M, Capellini G, Simmons M Y and Scappucci G 2013 *ACS Nano* **7**, 11310–11316.

10. Prucnal S, Rebohle L and Skorupa W 2017 *Materials Science in Semiconductor Processing*, **62**, 115-127.

11. Kim J, Bedell S W and Sadana D K 2012 *Appl. Phys. Lett.* **101**, 112107.

12. Milazzo R, et al. 2017 *Appl. Phys. Lett.* **110**, 011905 (2017).

13. Gallacher K, Velha P, Paul D J, MacLaren I, Myronov M and Leadley D R 2012 *Appl. Phys. Lett.* **100**, 022113.

14. Duan N et al.2016 *IEEE Trans. Electron Devices*, **63**, 4546.

15. Spann J Y, Anderson R A, Thornton T J, Harris G, Thomas S G Tracy C 2005 *IEEE Electron Device Lett.,* **26**, 151–153.

16. Lin J.-Y J, Roy A M and Saraswat K C 2012 *IEEE Electron Device Lett.,* **33**, 1541–1543.

17. Samarelli A, Frigerio J, Sakat E, Baldassarre L, Gallacher K, Finazzi M, Isella G, Ortolani M, Biagioni P and Paul D J 2016 *Thin Solid Films* **602**, 52–55.

18. Fang Y.-Y, Tolle J, Roucka R, Chizmeshya A V G, Kouvetakis J, D'Costa V R and Menéndez J 2007 *Appl. Phys. Lett.* **90**, 61915.

19. Contreras G, Compaan A and Axmann A 1983 *Journal de Physique Colloques*, **44 (C5)**, C5-193-C5-195.

20. El Kurdi M, Fishman G, Sauvage S and Boucaud P 2010 *J. Appl. Phys*. **107**, 013710.

21. Fan W J 2013 *J. Appl. Phys*. **114**, 183106.

22. Grzybowski G, Roucka R, Mathews J, Jiang L, Beeler R T, Kouvetakis J and Menéndez J 2011 *Phys. Rev. B* **84**, 205307.

23. Liu J, Sun X, Pan D, Wang X, Kimerling L C, Koch T L and Michel J 2007 *Opt. Express* **15**, 11272–7.

24. Jiang L, Gallagher J D, Senaratne C L, Aoki T, Mathews J, Kouvetakis J and Menéndez J 2014 *Semicond. Sci. Technol.* **29** 115028.

25. Massalski T B, Okamoto H, Subramanian P R, Kacprzak L (Eds.), Binary Alloy Phase Diagrams, ASM International, Materials Park, OH, 1990.

26. Guo Y, An X, Huang R, Fan C and Zhang X 2010 *Appl. Phys. Lett.* **96**, 143502.

27. Pfisterer H and Schubert K 1950 *Naturwissenschaften* **37**, 112.